

# Sub-parsec-scale Acceleration of the Radio Jet in the Powerful Radio Galaxy NGC 6251

Hiroshi SUDOU,<sup>1</sup> Yoshiaki TANIGUCHI,<sup>1</sup> Youichi OHYAMA,<sup>2</sup> Seiji KAMENO,<sup>2</sup>  
 Satoko SAWADA-SATO,<sup>2</sup> Makoto INOUE,<sup>2</sup> Osamu KABURAKI,<sup>1</sup> and Tetsuo SASAO<sup>2</sup>

<sup>1</sup>*Astronomical Institute, Graduate School of Science, Tohoku University, Aoba, Sendai 980-8578*

*E-mail (HS): sudou@astr.tohoku.ac.jp*

<sup>2</sup>*National Astronomical Observatory of Japan, 2-21-1 Osawa, Mitaka, Tokyo 181-8588*

(Received ; accepted )

## Abstract

In order to investigate the genesis of powerful radio jet, we have mapped the central 10 pc region of the nearby radio galaxy NGC 6251 with a 0.2 pc resolution using Very Long Baseline Interferometer (VLBI) at two radio frequencies, 5 GHz and 15 GHz, we have found the sub-parsec-scale counterjet for the first time in this radio galaxy. This discovery allows us to investigate the jet acceleration based on the relativistic beaming model.

**Key words:** galaxies: individual (NGC 6251) — galaxies: active — galaxies: jet — galaxies: nuclei — radio continuum: galaxies

## 1. Introduction

The powerful radio jets are observed in approximately ten percent of luminous AGN and their maximum lengths sometimes amount to  $\sim 1$  Mpc (Bridle, Perley 1984). Although global morphological properties give us very important information, very inner regions in the radio jets also provide hints for understanding the genesis of radio jets. The capability of Very Long Baseline Interferometry (VLBI) at radio frequency has been very useful in investigating such inner regions of relatively nearby radio galaxies (Zensus 1997). It has grown significantly since the launch of the space radio telescope HALCA (Highly Advanced Laboratory for Communications and Astronomy); a key element of the VLBI Space Observatory Program (VSOP) system (Hirabayashi et al. 1998; this volume). This has enabled us to investigate radio galaxies at the sub-milli arcsecond angular resolution, although the resolution depends on the radio frequency.

Since it is known that powerful radio jets are often emanated from the central engine of AGN at a relativistic speed, the inner region of radio jets is just a very exciting place. Since a pair of radio lobes are generally observed in the radio galaxies, the jet is believed to be intrinsically ejected in two opposite directions. However, although the approaching jet is enhanced by the Doppler beaming, the receding one (the counterjet) is significantly extinguished if the jet velocity is highly relativistic and is observed from a smaller viewing angle toward the jet. Indeed, in many radio galaxies, the counterjet is hardly seen in the

vicinity of the radio core. Since a typical distance of the radio jets resolved by VLBI is  $\sim 1$  pc inner region, this inner region is called as pc-scale jets (Zensus 1997).

NGC 6251 is one of apparently brightest powerful radio galaxies in the nearby universe and thus has been investigated extensively using VLBI as well as VLA (Very Large Array) (Waggett et al. 1977; Cohen, Readhead 1979; Perley et al. 1984; Jones et al. 1986; Jones, Wehrle 1994). So far these measurements failed to detect the pc-scale counterjet. If we could detect it, it will be possible to give many important observational constraints on the jet geometry and then the physical process of jet acceleration. If the jet acceleration would occur at a sub-pc region, we could detect the counterjet because the fading due to the Doppler beaming is still insignificant. In order to find evidence for such sub-pc-scale counterjet in NGC 6251, we have performed new high-resolution VLBI observations using HALCA. We use a distance to NGC 6251, 94.4 Mpc, which is determined with the use of a recession velocity to the galactic standard of rest,  $V_{\text{GSR}} = 7079 \text{ km s}^{-1}$  (de Vaucouleurs et al. 1991) and a Hubble constant  $H_0 = 75 \text{ km s}^{-1} \text{ Mpc}^{-1}$ . Note that 1 mas (milli arcsecond) corresponds to 0.48 pc at this distance.

## 2. Observations

NGC 6251 was observed at 5 GHz using VSOP on 30 April 1998 (10.1 h on-source) and at 15 GHz using VLBA (Very Long Baseline Array) on 2 June 1998 (9.3 h on-source). The VSOP system used in our observation

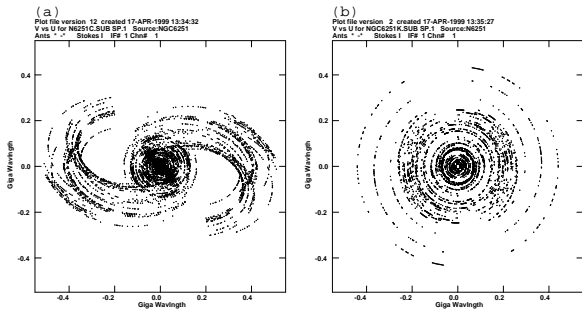


Fig. 1.. The  $uv$  coverages at 5 GHz (a) and at 15 GHz (b).

consists of HALCA, VLBA, and Effelsberg 100-m radio telescope near Bonn. Details of the observations are summarized in table 1. Since quality of the data taken at the Mauna Kea station of VLBA appeared to be poorer than those taken at the other stations, we flagged out the visibilities with the Mauna Kea station. The band width of the VSOP receivers is 32 MHz, divided into two IF bands, each of which has 128 channels at 5 GHz. The bandwidth of the VLBA receivers is also 32 MHz but divided into four IF bands each of which has 16 channels at 15 GHz. We used the source 1803+784 as a calibrator at both frequencies. Correlation processes have been carried out using the VLBA correlator at Socorro in New Mexico. The integration time at the correlator was 3 s. We used the NRAO AIPS package for fringe fitting and a-priori amplitude calibration. Image restoration via self-calibrations were made using DIFMAP. The resulting visibilities were coherently averaged for 30 s. The synthesized beam size of the two images are  $0.73 \times 0.34$  mas in  $PA = -9.2^\circ$  at 5 GHz and  $0.46 \times 0.38$  mas in  $PA = -13.4^\circ$  at 15 GHz with uniform weighting. In order to perform beam-size-matched comparison between 5 GHz and 15 GHz, we restored the two images with a same spatial resolution of  $0.50 \times 0.50$  mas. The  $uv$  coverages of the two observations are shown in figure 1.

### 3. Results

Our final maps at 5 GHz and 15 GHz are shown in figure 2a and 2b, respectively. The dynamic ranges are 160 for the 5 GHz map and 1400 for the 15 GHz map. In both maps, several knots are found within 10 mas (4.8 pc) from the each brightest peak. Analyzing the wiggling patterns in both frequencies, we obtain an opening angle of the jet,  $\phi \simeq 0.50^\circ \pm 0.29^\circ$ . It is remarkable that a counterjet-like feature can be seen in both maps although its spatial extension is only  $\approx 1$  mas. The most prominent knot in the 5 GHz map is seen at  $\approx 2.0$  mas (0.96 pc) away from the 5 GHz brightest peak. Its intensity is  $\approx$

26% of the 5 GHz core. This knot is found for the first time. It is also seen in the 15 GHz map. However, its angular distance from the 15 GHz brightest peak is  $\approx 2.3$  mas which is larger by 0.3 mas (0.14 pc) than that in the 5 GHz map.

Since any VLBI images have no information on the absolute position because of the self-calibration procedure, this difference makes it difficult to register the two images precisely. Since it is often observed that radio cores are optically thick even at those frequencies because of higher plasma densities, it is unlikely that the observed brightest peak positions always correspond to the real core position; here we assume that the very center of the active nucleus, i.e., the central engine is enshrouded by the VLBI core. On the other hand, knots are thought to be optically thin and thus their brightness distributions show more realistic distributions of plasma. Therefore, it is better to register the two images using the spatial and morphological information of knots between the two maps.

Here we apply two new methods for the registration. The first one is to analyze the correlation function between intensity profiles of the radio jet at the two frequencies. The correlation function exhibits the maximum correlation coefficient  $C_{\text{int}} \simeq 0.98$  at an offset of  $\Delta_{\text{int}} \simeq 0.30 \pm 0.0025$  mas, indicating that the peak at 5 GHz is shifted by  $\Delta_{\text{int}}$  to the jet direction from that at 15 GHz (figure 3a). The second method is to analyze the correlation function between wiggle patterns of the radio jet at the two frequencies. This analysis gives an offset of  $\Delta_{\text{wig}} \simeq 0.10 \pm 0.24$  mas with the maximum correlation coefficient of  $C_{\text{wig}} \simeq 0.34$  (figure 3b). Since an offset of  $\Delta_{\text{int}}$  is in good agreement with that of  $\Delta_{\text{wig}}$  within their errors, we adopt a  $\Delta = 0.3$  mas as the best offset. Using this offset, we register the two images and make a spectral index image of the radio jet of NGC 6251 shown in figure 2c. Here the spectral index  $\alpha$  is defined as  $S_\nu \propto \nu^\alpha$ . It is shown that the core region has an inverted spectrum with  $\alpha \simeq 1.2$  and thus it appears optically thick. On the other hand, the spectral index of the jet ranges  $-1$  and  $-0.5$  and thus the jet is optically thin. The counterjet-like feature has a spectral index of  $\simeq -0.5$  and thus appears to be optically thin. This ensures that it is the counterjet. Its intensity level is  $\sim 10\sigma_{\text{rms}}$  at 5 GHz and  $\sim 40\sigma_{\text{rms}}$  at 15 GHz, where  $\sigma_{\text{rms}}$  is the one sigma root-mean-square noise in each map. Therefore, we conclude that this is the real counterjet. Curiously, the morphology of the counterjet is slightly different between the two images, i.e., two ridge lines can be seen only at 15 GHz. Although it is difficult to understand such a morphological difference, we confirmed that one of ridge lines at 15 GHz corresponds to the counterjet at 5 GHz.

Table 1. Observations.

Observations	$\nu$ (GHz)	Stations	Peak Int. (Jy/beam)	RMS noise (mJy/beam)	Dynamic Range
1998 Apr. 30	5	VLBA, HALCA*, EB†	0.13	0.82	160
1998 Jun. 02	15	VLBA	0.34	0.24	1400

\*Highly Advanced Laboratory of Communication and Astronomy

†Effelsberg 100-m telescope

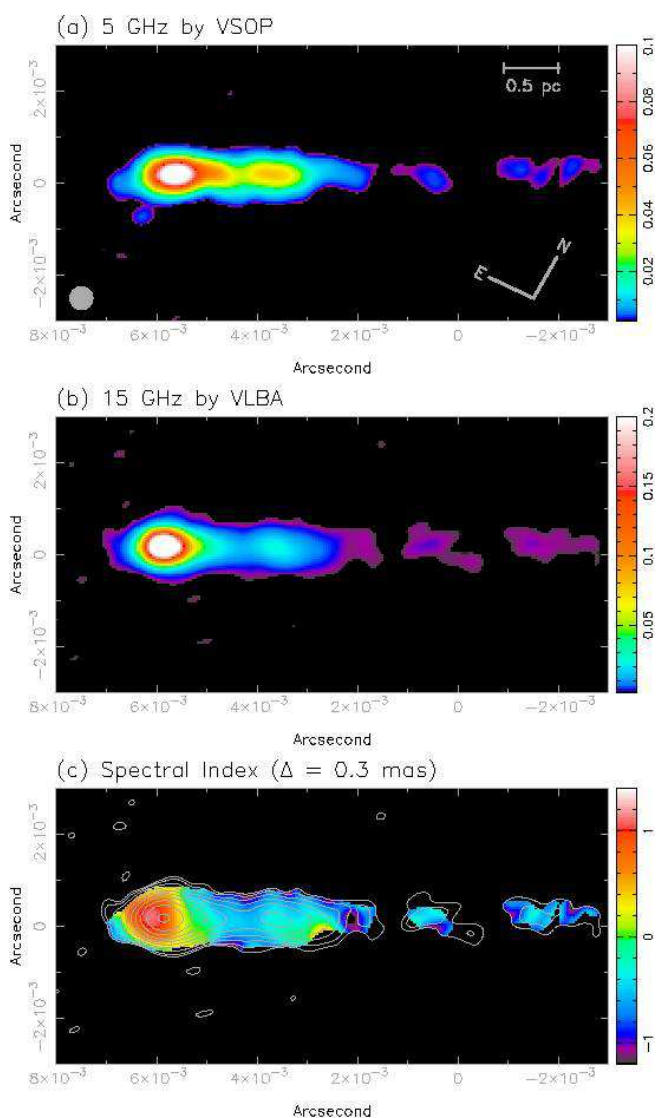


Fig. 2. The images of NGC 6251 at 5 GHz (a) and at 15 GHz (b). The spectral index map together with the 15 GHz contour image is also shown in (c). All the images rotated clockwise on the sky by  $28.4^\circ$ .

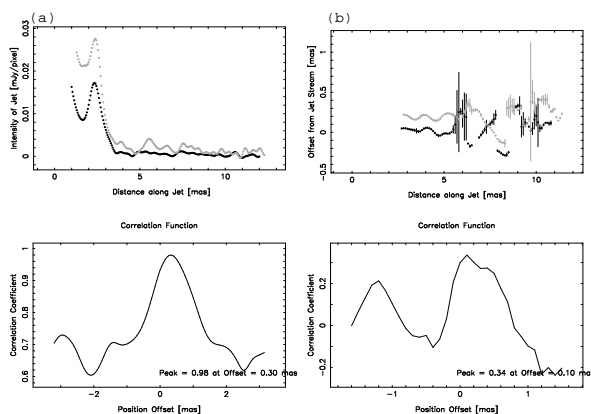


Fig. 3. *Top*: Intensity profiles (a) and wiggling patterns (b) at 5 GHz (grey circle) and 15 GHz (filled circle). They are already registered. *Bottom*: Correlation coefficient as a function of offset.

## 4. Discussion

### 4.1. The Absorption Model at the Core

The inverted spectrum in the core implies that there is a strong absorption at 5 GHz. This may explain why the brightest position at 5 GHz does not coincide with that at 15 GHz. In general, such absorption in the radio jet is caused either by free-free absorption or by synchrotron self-absorption. Since it seems quite likely that a plasma halo (or ring) surrounds the central engine, the free-free absorption seems to be a dominant absorption mechanism, i.e., the flux density at 5 GHz is more significantly absorbed by the free-free absorption than the 15 GHz brightest peak flux.

Free-free absorption models give a relation  $S_\nu = S_0 \nu^{\alpha_0} \exp[-\tau_0 \nu^{-2.1}]$ . Accordingly, we obtain,

$$\tau_{\text{obs}} = \frac{\alpha_5^{15} - \alpha_0}{0.0279} \left( \frac{\nu}{\text{GHz}} \right)^{-2.1}, \quad (1)$$

where  $\alpha_5^{15}$  is the spectral index between 5 and 15 GHz and  $\alpha_0$  is the intrinsic spectral index of the jets. Using

$\alpha_5^{15} = 1.2$ ,  $\alpha_0 = -0.5$ , and  $\nu = 5$  GHz, we obtain  $\tau_{\text{obs}} = 2.4$ .

A question arises as how the absorbing material is distributed around the central engine at a sub-pc-scale. Since we do not know the true situation, we will investigate the following three absorption models: (1) a spherical absorber model, (2) an optically-thick disk model, and (3) an optically-thin disk model.

#### 4.1.1. The spherical absorber model

First, we investigate a spherical absorber model because this model is the simplest one. We assume that the core is surrounded by a plasma sphere with a radius of  $a$  and the radio emission from the inner part of the jets (i.e., both the jet and the counterjet) suffer from the free-free absorption. We show this model schematically in figure 4. In this model, we adopt the 15 GHz brightest peak as the core in which the central engine resides. The approaching jet escapes from the plasma sphere at a projected distance of  $x = a \times \sin \theta_{\text{jet}}$  and thus the optical depth becomes to be small (i.e.,  $\tau_{\text{obs}} < 1$ ) here. On the other hand, although the counterjet escapes the sphere at  $x = -a \times \sin \theta_{\text{jet}}$ , it suffers the effect of free-free absorption until  $x = -a$ . It is also noted that the path length is longest at  $x = -a \times \sin \theta_{\text{jet}}$ . As shown in figure 4, we define the following projected distances;  $X_{\text{jet}} = X_{\text{peak}} = a \times \sin \theta_{\text{jet}}$  and  $X_{\text{cjet}} = a$ . Then we are able to estimate  $\theta_{\text{jet}}$ ,

$$\theta_{\text{jet}} = \sin^{-1} \left( \frac{X_{\text{jet}}}{X_{\text{cjet}}} \right) \quad (2)$$

In figure 5, we show the observed spectral index variation along the radio jet. The opacity is assumed to be proportional to the path length through the plasma sphere. The region with an inverted spectrum is considered to be optically thick for the free-free absorption ( $\tau_{\text{obs}} > 1$ ) while that with a normal spectrum is optically thin. We adopted that  $\tau_{\text{obs}} = 1$  when the jets escape from the sphere. From equation (1), note that  $\tau_{\text{obs}} = 1$  at 5 GHz corresponds to  $\alpha_5^{15} = 0.2$  and that  $\tau_{\text{obs}}$  at 15 GHz is always smaller than unity in our observations. Therefore, from figure 5, we estimate  $X_{\text{peak}} \approx 0.20$  mas,  $X_{\text{jet}} \approx 0.25$  mas, and  $X_{\text{cjet}} \approx 0.75$  mas. Then we obtain  $\theta_{\text{jet}} \simeq 19^\circ$ . In the previous VLBI measurements of the pc-scale jet of NGC 6251, Jones (1986) obtained  $\theta_{\text{jet}} \leq 45^\circ$  using the upper limit of the counterjet flux. Our estimate appears consistent with their result. Although our simple model suggests  $X_{\text{jet}} = X_{\text{peak}}$ , the observation results in  $X_{\text{jet}}/X_{\text{peak}} \approx 1.3 \neq 1$ . This may be caused by plasma density fluctuation in the actual radio core of NGC 6251. If we adopt the observed value of  $X_{\text{jet}}$  instead of  $X_{\text{peak}}$ , we obtain  $\theta_{\text{jet}} \simeq 15^\circ$ .

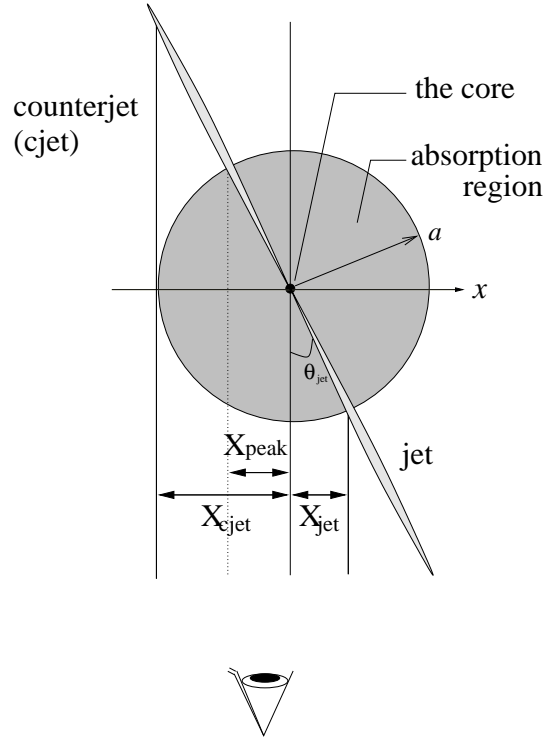


Fig. 4.. A schematic illustration of the spherical absorber model in NGC 6251.

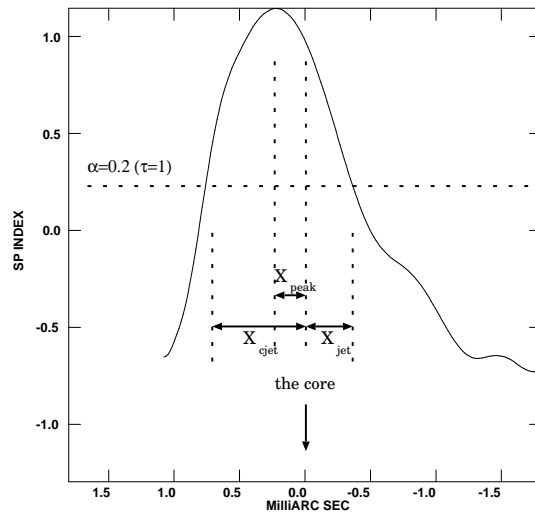


Fig. 5.. Spectral index variation along the jet near the core.

#### 4.1.2. The optically-thick disk model

Although the spherical absorber model is useful for estimating the jet viewing angle, it is too simple to determine the detailed environment of the radio core. Recently, it has been reported that a very narrow gap near the core of the radio jet in NGC 4261 is attributed to the absorption by a geometrically thin, nearly edge-on accretion disk (Jones et al. 2000). In this case, the central engine may be powered by gas accretion at a sub-Eddington accretion rate. It is expected that an accretion structure consists of an optically-thin, advection-dominated accretion flow (ADAF) in the central region and a geometrically thin accretion disk surrounding it (e.g., Narayan et al. 1998). This idea can be applicable to the case of NGC 6251.

We consider that the central black hole is surrounded by such a tenuous plasma or coronal region which is related to ADAF, and that a relatively dense outer disk causes a strong free-free absorption. In this model, the strongest absorption should be observed at the inner edge of the outer disk. Therefore, we identify the location of the maximum absorption at 5 GHz with the inner edge. If the jet viewing angle  $\theta_{\text{jet}} = 30^\circ$  (see Sudou, Taniguchi 2000), then we obtain the linear distance of the inner edge,  $r_{\text{peak}} \equiv X_{\text{peak}}/\cos\theta \approx 3.3 \times 10^{17}$  cm. This model is shown schematically in figure 6.

According to the usual understanding of accretion disks (Narayan et al. 1998), we regard the outer disk as the optically-thick disk (Shakura, Sunyaev 1973). Since the density and the temperature are low in this outer disk, the free-free absorption may be dominant over the electron scattering. Following Shakura and Sunyaev (1973), the half thickness of the disk  $H$ , the particle density  $n$ , and the electron temperature  $T$  are given by,

$$H = 4.0 \times 10^{10} \alpha_{\text{vis}}^{-1/10} \dot{m}^{3/20} m^{9/10} \hat{r}^{9/8} \text{ cm}, \quad (3)$$

$$n = 2.1 \times 10^{21} \alpha_{\text{vis}}^{-7/10} \dot{m}^{11/20} m^{-7/10} \hat{r}^{-15/8} \text{ cm}^{-3}, \quad (4)$$

and

$$T = 9.8 \times 10^6 \alpha_{\text{vis}}^{-1/5} \dot{m}^{3/10} m^{-1/5} \hat{r}^{-3/4} \text{ K}, \quad (5)$$

respectively, where  $\alpha_{\text{vis}}$  is the viscosity parameter, and  $m$  is the black hole mass,  $\dot{m}$  is the mass accretion rate, and  $\hat{r}$  is the radial distance. The latter three parameters are scaled for a typical AGN as  $m \equiv M_{\text{BH}}/10^8 M_\odot$ ,  $\dot{m} \equiv \dot{M}/\dot{M}_{\text{crit}}$  ( $\dot{M}_{\text{crit}} \equiv L_{\text{Edd}}/0.1c^2 \sim 1.5 \times 10^{26} m \text{ g s}^{-1}$ ), and  $\hat{r} \equiv r/r_g$  ( $r_g \equiv 2GM/c^2 \sim 3.0 \times 10^{13} m \text{ cm}$ ). For NGC 6251, we adopt  $m = 8$  (Ferrarese, Ford 1999),  $\dot{m} = 0.001$  (Birkinshaw, Worrall 1994), and  $\hat{r} = \hat{r}_{\text{peak}} = 1.4 \times 10^3$ . Assuming  $\alpha_{\text{vis}} = 0.1$ , we obtain,  $H = 4.0 \times 10^{14}$  cm,  $n = 7.0 \times 10^{13} \text{ cm}^{-3}$ , and  $T = 5.5 \times 10^3$  K. Although  $H$  and  $T$  are reasonable compared with observations,  $n$  is too large as to give a very high opacity of  $\tau \sim 10^{16}$  at 5 GHz. Therefore, this model fails to explain the observational properties of NGC 6251.

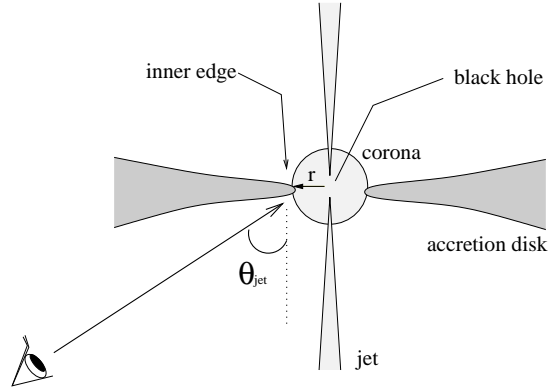


Fig. 6.. A schematic illustration of the absorption disk model in NGC 6251.

#### 4.1.3. The optically-thin disk model

Next, we attempt to explain  $\tau_{\text{obs}}$  adopting an optically-thin disk model in which the viscous heating is balanced by the free-free cooling. Adopting the cooling rate of  $1.2 \times 10^{21} m_p^2 n^2 T^{1/2} H \text{ erg s}^{-1} \text{ cm}^{-2}$  (Kato et al. 1998), we obtain,

$$H = 5.8 \times 10^{12} \alpha_{\text{vis}}^{-1/2} \dot{m}^{1/4} m^1 \hat{r}^{9/8} \text{ cm}, \quad (7)$$

$$n = 5.3 \times 10^{13} \alpha_{\text{vis}}^{1/2} \dot{m}^{1/4} m^{-1} \hat{r}^{-15/8} \text{ cm}^{-3}, \quad (8)$$

$$T = 1.0 \times 10^{12} \alpha_{\text{vis}}^{-1} \dot{m}^{1/2} m^0 \hat{r}^{-3/4} \text{ K}. \quad (9)$$

Adopting the same parameter values as those in section 4.1.2, we obtain  $H = 9.0 \times 10^{16}$  cm,  $n = 4.7 \times 10^5 \text{ cm}^{-3}$ , and  $T = 1.4 \times 10^9$  K for NGC 6251. The derived temperature of  $T \sim 10^9$  K is much higher than that of  $\sim 10^4$  K assumed in the model of Jones et al. (2000).

In view of the resulting high electron temperature, the cooling in this situation may be dominated by the inverse Compton scattering rather than by free-free radiation. The model suitable for such a condition may be that of Shapiro et al. (1976) which adopts that the radiation cooling is dominated by inverse Compton scattering. In fact, the expected free-free optical depth in our model is only  $\sim 10^{-6}$ . Therefore, we conclude that this model is unsuitable for the absorption mechanism of NGC 6251.

#### 4.1.4. Summary of the absorption models

The simplest spherical absorption model provides the plausible explanation for the observed absorption properties. On the other hand, the optically-thick and optically-thin disk models fail to explain the observations, although the presence of the disk structure would be naturally expected around the central engine. It will be necessary to seek for other types of outer accretion-disk models which are consistent with the observations.

#### 4.2. Velocity of the Jet

Adopting the so-called Doppler beaming model (e.g., Ghisellini et al. 1993), we estimate the jet velocity using the observed jet-counterjet intensity ratio; i.e., if the jet of NGC 6251 is intrinsically two-directional symmetric, the observed intensity asymmetry between the jet and counterjet can be attributed to the Doppler beaming. The jet-counterjet intensity ratio  $R$  is related to both the intrinsic jet velocity  $v_{\text{jet}}$  and the viewing angle  $\theta_{\text{jet}}$  toward the jet by the formula

$$R = \left[ \frac{1 + \beta_{\text{jet}} \cos \theta_{\text{jet}}}{1 - \beta_{\text{jet}} \cos \theta_{\text{jet}}} \right]^{3-\alpha_0}, \quad (10)$$

where  $\beta_{\text{jet}} = v_{\text{jet}}/c$ . Using the intensity profiles of both 5 GHz and 15 GHz along the jet direction, we have measured  $R$  and plot them in figure 7. Note that the core component ( $|x| \leq 0.5$  mas) is not used in this analysis. Although the estimated value of  $R$  at 1.05 mas from the core is the same at both frequencies, that within 0.8 mas from the core is higher at 5 GHz than at 15 GHz. Since this is probably due to severer absorption at 5 GHz than at 15 GHz, the value of  $R$  at 15 GHz appears to be more reliable. It is shown that  $R$  increases with increasing projected distance from the core. If this increase is caused mainly by the Doppler beaming, it is suggested that  $\beta_{\text{jet}}$  and/or  $\theta_{\text{jet}}$  increase with increasing distance. Since it is unlikely that  $\theta_{\text{jet}}$  varies significantly at such a small scale, it seems reasonable to conclude that the increase of  $R$  is attributed to the increase in  $\beta_{\text{jet}}$ . This can be interpreted as possible evidence for the acceleration at the sub-pc-scale radio jet. Using equation (9) and assuming  $\theta_{\text{jet}} = 30^\circ$ , we show that the jet is accelerated from  $\beta_{\text{jet}} \approx 0.13$  at 0.55 mas to  $\beta_{\text{jet}} \approx 0.42$  at 1.05 mas. The results are summarized in table 2. These angular distances correspond to the linear distances of  $\approx 0.30$  pc and  $\approx 0.58$  pc, respectively.

If the jet acceleration is effectively made at sub-pc-scale region, the jet velocity becomes relativistic at radial distance of  $\sim 1$  pc. If the sub-pc-scale acceleration is a general property in most radio galaxies, it seems difficult to detect pc-scale counterjets. It will be very important to observe sub-pc-scale jets at higher frequency because the effect of absorption is negligibly small.

Since the kinetic energy of a particle with a mass of  $m$  at a relativistic velocity of  $v$  is given as  $E = m\gamma v^2 = m\gamma\beta^2 c^2$  where  $\gamma = (1 - \beta^2)^{-1/2}$ , the kinetic energy gain from  $\beta = 0.1$  to  $\beta = 0.4$  per unit mass is  $\Delta E/m \sim 3 \times 10^{16}$  J kg $^{-1}$ . This corresponds to the kinetic energy of  $\sim 200$  keV for an electron and to that of  $\sim 300$  MeV for a proton. Therefore, it is suggested that the jet acceleration region found in NGC 6251 is related to the  $\gamma$ -ray emitting region. This may explain why  $\gamma$ -ray loud AGNs tend to be associated with radio-loud AGNs if such acceleration occurs commonly in radio galaxies (Shrader et al. 1995).

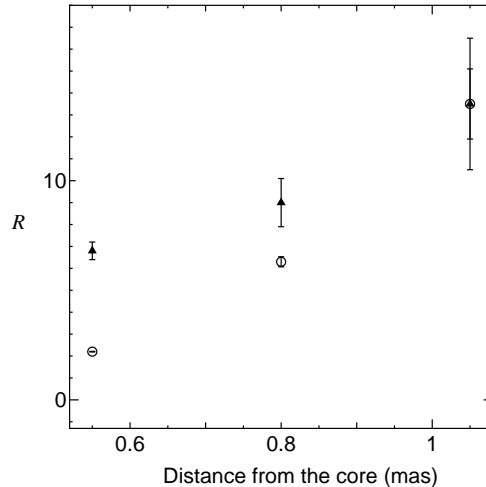


Fig. 7.. The jet-counterjet ratio  $R$  as a function of the projected distance from the core. The filled triangle and open circle indicate obtained  $R$  at 5 GHz and 15 GHz, respectively.

## 5. Conclusions

We discussed high-resolution images of NGC 6251 at 5 GHz and 15 GHz. From the analyses of the intensity profile and the wiggling pattern, we register the two images and obtain the spectral index image. It shows the counterjet which has an optically-thin spectrum. In order to explain the position difference between the core and the absorption peak, we adopt the simple spherical absorption model, and show the possibility that the jet viewing angle can be obtained from only the spectral index distribution. Although we also attempt to adopt the free-free absorption by an accretion disk model, both optically thick and thin disk models based on the  $\alpha$ -viscosity cannot explain the observed opacity.

The jet-counterjet intensity ratio analysis shows that the radio jet of NGC 6251 is accelerating from  $0.13 c$  at the linear radial distance of  $r \approx 0.30$  pc to  $0.42 c$  at  $r \approx 0.58$  pc. This provides the first direct evidence for the sub-pc-scale acceleration of the radio jet in NGC 6251.

We would like to thank to staff of the VLBA and the VSOP for their kind help of the observations. We also wish to thank D. Jones and H. Hirabayashi for their useful comments and encouragement. This work was financially supported in part by Grant-in-Aids for the Scientific Research (Nos. 10044052, and 10304013) of the Japanese Ministry of Education, Culture, Sports, and Science. HS was supported by the Grant-in-Aid for JSPS Fellows by Ministry of Education, Culture, Sports, and Science.

Table 2. The jet/counterjet intensity ratio.

Distance (mas)	$R_5^*$	$R_{15}^\dagger$	$\beta_{\text{jet}}^\ddagger$
0.55 .....	6.8±0.4	2.2±0.015	0.13±0.0014
0.80 .....	9.0±1.1	6.3±0.23	0.30±0.0053
1.05 .....	13.5±3.0	13.5±1.6	0.42±0.017

\*  $R$  at 5 GHz†  $R$  at 15 GHz‡ Assuming  $\theta_{\text{jet}} = 30^\circ$ 

## References

- Birkinshaw M., Worrall D.M. 1993, ApJ 412, 568  
 Bridle A.H., Perley R.A. 1984, ARA&A 22, 319  
 Cohen M.H., Readhead A.C.S. 1979, ApJL 233, L101  
 de Vaucouleurs G., de Vaucouleurs A., Corwin, C.Jr., Buta R.J., Paturel G., Fouqué P. 1991, in Third Reference Catalogue of Bright Galaxies, (Springer-Verlag)  
 Ferrarese L., Ford H.C. 1999, ApJ 515, 583  
 Ghisellini G., Padovani P., Celotti A., Maraschi L. 1993, ApJ 407, 65  
 Hirabayashi H., Hirose H., Kobayashi H., Murata Y., Edwards P.G., Fomalont E.B., Fujisawa K., Ichikawa T. et al. 1998, Science 281, 1825  
 Jones D.L., Unwin S.C., Readhead A.C.S., Sargent W.L.W., Seielstad G.A., Simon R.S., Walker R.C., Benson J.M. et al. 1986, ApJ 305, 684  
 Jones D.L. 1986, ApJL 309, L5  
 Jones D.L., Wehrle A.E. 1994, ApJ 427, 221  
 Jones D.L., Wehrle A.E., Meier D.L., Piner G.B. 2000, ApJ 534, 165  
 Kato S., Fukue J., Mineshige S. 1998, in Black-Hole Accretion Disks (Kyoto Univ. Press) p248  
 Narayan R., Mahadevan R., Quataert E. 1998, in Theory of Black Hole Accretion Disks, ed M.A. Abramowicz, G. Björnsson, J.E. Pringle (Cambridge Univ. Press) p148  
 Perley R.A., Bridle A.H., Willis A.G. 1984, ApJS 54, 291  
 Shakura N.I., Sunyaev R.A. 1973, A&A 24, 337  
 Shapiro S.L., Lightman A.P., Eardley D.M. 1976, ApJ 204, 187  
 Shrader C.R., Gehrels, N. 1995, PASP 107, 606  
 Sudou H., Taniguchi Y. 2000, AJ in press  
 Urry C.M., Padovani P. 1995, PASP 107, 803  
 Waggett P.G., Warner P.J., Baldwin J.E. 1977, MNRAS 181, 465  
 Zensus J.A. 1997, ARA&A 35, 607

This figure "Sudou\_fig2.jpg" is available in "jpg" format from:

<http://arxiv.org/ps/astro-ph/0008173v1>